Inorganic Chemistry

Article

pubs.acs.org/IC

Role of Spin State and Ligand Charge in Coordination Patterns in Complexes of 2,6-Diacetylpyridinebis(semioxamazide) with 3d-Block Metal Ions: A Density Functional Theory Study

Stepan Stepanović,[†] Ljubica Andjelković,[†] Matija Zlatar,[†] Katarina Andjelković,[‡] Maja Gruden-Pavlović,*[,‡] and Marcel Swart*[,§,⊥]

[†]Center for Chemistry, IHTM and [‡]Faculty of Chemistry, University of Belgrade, Studentski trg 12−16, Belgrade, Serbia

[§]Institut de Química Computacional i Catàlisi (IQCC) and Departament de Química, Universitat de Girona, Campus Montilivi, Facultat de Ciències, 17071 Girona, Spain

[⊥]Institució Catalana de Recerca i Estudis Avançats (ICREA), Pg. Lluís Companys 23, 08010 Barcelona, Spain

Supporting Information

ABSTRACT: We report here a systematic computational study on the effect of the spin state and ligand charge on coordination preferences for a number of 3d-block metal complexes with the 2,6-diacetylpyridinebis(semioxamazide) ligand and its mono- and dianionic analogues. Our calculations show excellent agreement for the geometries compared with the available X-ray structures and clarify some intriguing experimental observations. The absence of a nickel complex in seven-coordination is confirmed here, which is easily explained by inspection of the molecular orbitals that involve the central metal ion. Moreover, we find here that changes in the spin state lead to completely different coordination modes, in contrast to the usual situation that different spin states mainly result in changes in the metal−ligand bond lengths. Both effects result from different occupations of a combination of π- and σ-antibonding and nonbonding orbitals.

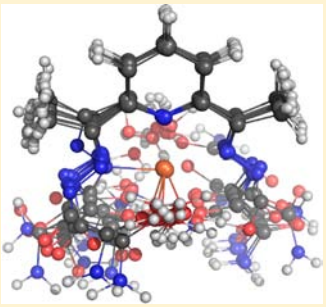

INTRODUCTION

Rapid progress in computational science, combined with advances in the development of electronic structure theory, has made computational chemistry an inseparable partner for experiments in recent years.[1−4] From a broad palette of electronic structure methods, density functional theory (DFT) emerged in the mainstream of quantum-chemical methods because of its good compromise between the accuracy of the results and the computational efficiency. This is true for organic chemistry,[5−10] but the advantages of DFT are still greater for transition-metal compounds,[11,12] where ligands cannot always be considered innocent bystanders.[13−15] Furthermore, there is no need to emphasize the importance of coordination compounds and the beauty of their rich stereochemistry and reactivity. However, most coordination compounds studied by theory are those with coordination numbers of 6[16,17] and 4,[18−20] even though in the past decades the interest in other coordination polyhedra has increased significantly because of their possible applications in biology and chemistry.[21−23]

Complexes of polydentate acylhydrazone ligands with d metals are particularly interesting because they have remarkable structural features that lead to a diversity of potential applications.[24−26] Among many others, 2,6-diacetylpyridinebis(semioxamazide) (H_2dapsox) and its monoanionic (Hdapsox) and dianionic (dapsox) forms are conformationally flexible ligands. Moreover, they have a large number of potential donor atoms (see Figure 1) and hence display versatile behavior in metal coordination, the exact nature of which depends on the reaction conditions. The mode of coordination appears to be governed by the nature of the central metal atom, the charge of the ligand, and the presence of other species able to compete for the coordination pockets.[27] Interestingly, the $H_n$dapsox ligands (n = 0, 1, 2) enable the formation of pentagonal-bipyramidal complexes (PBPY-7) with some 3d elements, even though seven-coordinate complexes are usually more common with large (d-block) metal ions. Until now, 3d metal PBPY-7 complexes have been isolated and characterized for the H_2dapsox ligand with Mn^{II},[28] Fe^{II},[29] Co^{II},[30] and Zn^{II}[28] and for Hdapsox and dapsox with Fe^{III}[31,32] and Co^{II}.[30,33] Other

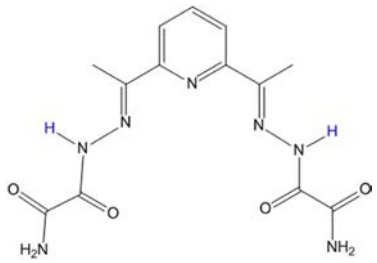

Figure 1. Schematic representation of the H_2dapsox ligand. Its mono- and dianionic forms are obtained primarily by dissociation of the hydrogen atoms indicated in blue.

Received: July 8, 2013
Published: November 19, 2013

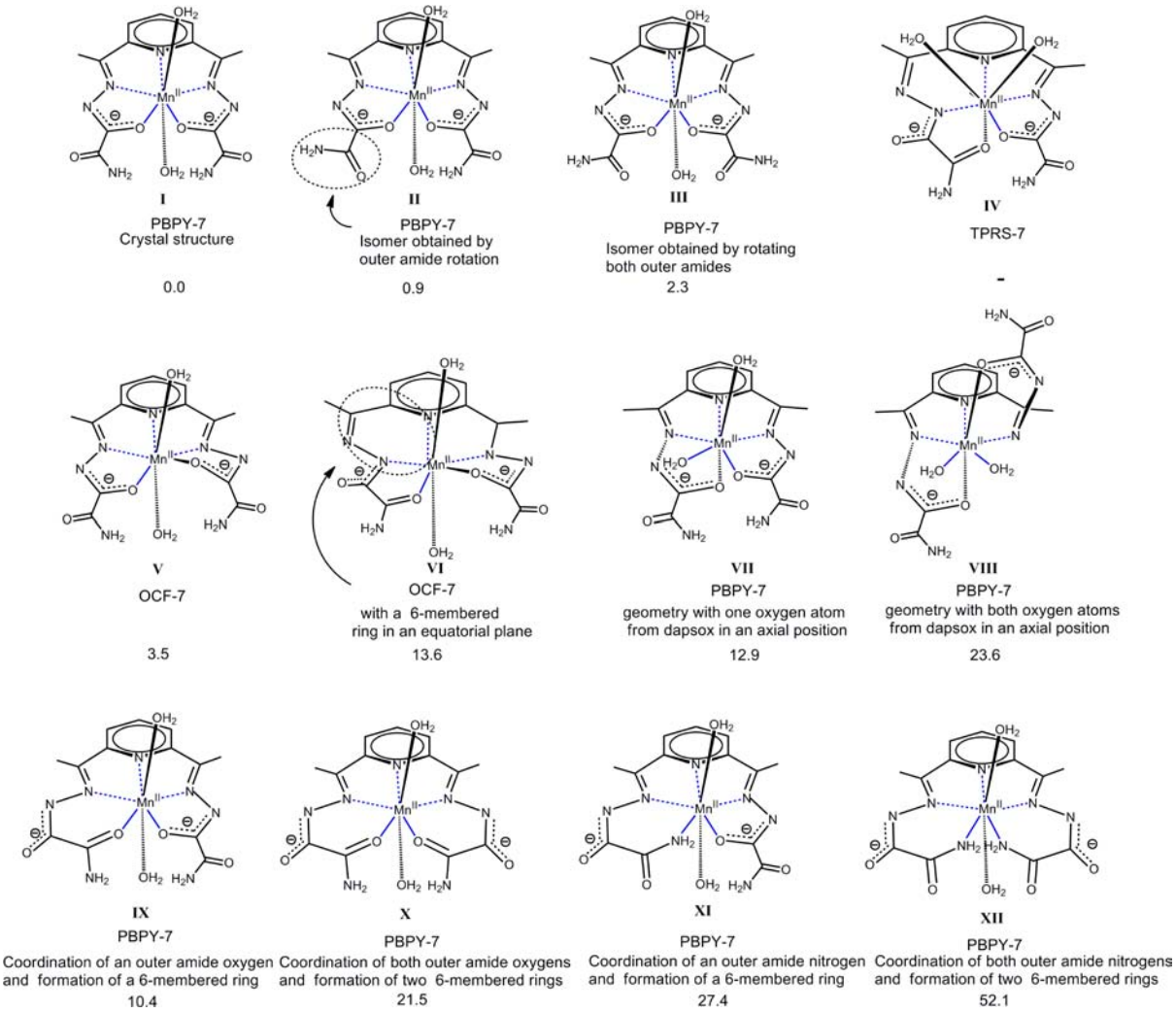

Figure 2. Possible general isomeric structures for $[M(H_ndapsox)(H_2O)_2]^q$. For $[Mn^{II}(dapsox)(H_2O)_2]$, relative energies (OPBE/TZP//LDA/TZP; kcal·mol^{-1}) are compared to those of the most stable isomer **I**; bonds that lie in the equatorial plane are labeled in blue.

geometries are also possible: an octahedral environment is found for $[Fe^{III}(dapsox)Cl]$[34] and $[Ni^{II}(Hdapsox)(MeOH)_2]ClO_4$,[32] while with dapsox, Ni^{II} forms a square-planar complex.[35] Furthermore, the di- and monoanionic forms enable the formation of square-pyramidal (SPY-5) complexes with Cu^{II}[32,36] and Fe^{III}.[34] Therefore, these ligands act as ligands of changeable dentation and exhibit a stereochemical diversity, especially with respect to coordination numbers and/or geometries observed for various d metal ions.

A characteristic feature of open-shell transition-metal ions in general is that several electronic configurations are accessible that may give rise to a number of different spin states, where the preferred one is determined by the ligand-field strength. In the case of the $H_n$dapsox ligand, this might be governed by the degree of (de)protonation.[14,37,38] The calculation of spin-state energies has turned out to be quite a challenge for computational methods,[14] in particular for density functionals. Early pure functionals like LDA,[39−42] BP86,[43,44] BLYP,[43,45] or PBE[46] have a tendency to favor low-spin states,[47] while hybrid functionals (B3LYP,[48] PBE0,[46,49] and M06-2X[50]) have a tendency to favor high-spin states[51] because of inclusion of a portion of Hartree−Fock exchange in these hybrid functionals. The situation changed completely through the application of more appropriate functionals like OPBE,[38,46,52,53] SSB-D[54] (and it successor S12g[55]), and TPSSh.[56] A recent study,[55] however, showed that long-range-corrected hybrid functionals [with 100% (long-range) Hartree−Fock exchange] could also be used reliably for providing the ground state of two related iron(II) complexes (monopyridylmethylamine $Fe^{II}(amp)_2Cl_2$ and dipyridylmethylamine $[Fe^{II}(dpa)_2]^{2+}$), given that the former has a high-spin ground state and the latter a low-spin ground state. The combination of these two complexes was shown[38,55] to be a critical test for computational methods.

To the best of our knowledge, and in spite of many experimental studies,[29,57−59] there are only few theoretical attempts that have tried to rationalize the structure and electronic properties of 3d metal complexes with H_2dapsox and its anionic forms.[22,23,25,60] Because these complexes represent mimics of superoxide dismutase (SOD) and ditopic receptors for lithium salts, they are of the utmost importance, and hence detailed kinetic and mechanistic experimental studies were reported previously.[29,57−61] Recently, time-dependent DFT (TDDFT) and semiempirical calculations were performed in order to rationalize the UV−vis spectra of the SOD mimics redox pair $[Fe^{III}(dapsox)(H_2O)_2]^+$ and $[Fe^{II}(H_ndapsox)(H_2O)_2]^{n+}$, explaining the nature of correctly tuned redox potentials in catalytic superoxide disproportionation.[25] However, it is still not clear why the experimentally observed

dx.doi.org/10.1021/ic401752n | Inorg. Chem. 2013, 52, 13415−13423

complexes are in a particular coordination geometry and, even less, what the roles are of the ligand charge and spin state of the 3d metal on these geometries. Thus, in order to enhance our understanding of these coordination preferences, we have performed a systematic DFT study of complexes of some 3d-block metal ions with $H_n$dapsox ligands. With these calculations, we have elucidated how the chelation properties of the ligands influence the stability of different geometries around the metal ions, which is achieved through different donor atoms as well as variation in the orbital occupations of the metal ions.

COMPUTATIONAL DETAILS

The calculations using the unrestricted formalism have been performed with the Amsterdam Density Functional (ADF) program package,[62−64] versions 2012.01/2013.01. Molecular orbitals (MOs) were expanded in an uncontracted set of Slater-type orbitals (STOs),[65] of triple-ζ quality containing diffuse functions plus one set of polarization functions (TZP). Geometry optimizations of all investigated structures were performed with the local density approximation (LDA).[39−41] Geometry optimizations have also been performed using generalized gradient approximation (GGA) functionals consisting of OPTX[52] for exchange and PBE[46] for correlation (OPBE[53]) on a carefully selected subset of the investigated complexes. Default integration and gradient convergence criterions were used. Subsequently, single-point-energy calculations were performed on the LDA- and OPBE-optimized geometries using either OPBE (for LDA geometries) or dispersion-corrected functionals: SSB-D,[54,66] which has so far shown to be very accurate for spin states,[67] and its recently reported successor S12g.[55] In order to check the possible influence of an environment, we also performed single-point calculations with a dielectric continuum model (COSMO)[68−70] (using water as a solvent), as implemented in ADF,[71,72] with the OPBE, SSB-D, and S12g functionals (on LDA geometries). The examined seven-coordinated complexes are described by the general formula $[M(H_n\text{dapsox})(H_2O)_2]^q$, where q = 0, 1, 2, 3, n = 0, 1, 2, and M = Mn^{II}, Fe^{II}/Fe^{III}, Co^{II}, Ni^{II}, Zn^{II}, while five-coordinated complexes are denoted by $[M(H_n\text{dapsox})L]^q$, q = −1, 0, 1, 2, n = 0, 1, L = H_2O, Cl, and M = Fe^{III}, Cu^{II}. For all d-block metal complexes, the geometry optimization is carried out for all accessible spin states separately: S = $^1/_2$, $^3/_2$, and $^5/_2$ for Mn^{II}, S = $^1/_2$, $^3/_2$, and $^5/_2$ for Fe^{III}, S = 0, 1, and 2 for Fe^{II}, S = $^1/_2$ and $^3/_2$ for Co^{II}, S = 0 and 1 for Ni^{II}, S = $^1/_2$ for Cu^{II}, and S = 0 for Zn^{II}.

RESULTS AND DISCUSSION

Stereochemistry of Seven-Coordinate Complexes. The most commonly observed coordination polyhedra in seven-coordinated transition-metal complexes are pentagonal bipyramid (PBPY-7), capped octahedron (OCF-7), and capped trigonal prism (TPRS-7);[27,73] see Figure 2. However, if the crystal structure is not determined, unambiguous experimental assignment of coordination polyhedra in seven-coordinated complexes is difficult because one structure may resemble more than one reference polyhedral, hence the need for a computational study of these complexes. The H_2dapsox ligand studied here has 11 potential ligator atoms (see Figure 1), some of which are mutually exclusive. This, together with the flexibility of both side chains attached to the pyridine ring, creates quite a diversified stereochemistry[36] with respect to the possible coordination modes, which could be summarized as follows: isomer **I** corresponds to the PBPY-7 X-ray-determined structures of the investigated complexes (vide supra),[29−31] while isomers **II** and **III** might be quoted as rotamers of isomer **I**.

The remaining isomeric structures of PBPY-7 have a different type, or positioning, of ligator atoms. In isomers **VII** and **VIII**, the dapsox ligand is not planar and its side chains occupy axial positions. When the dapsox ligand is in a planar conformation, there are two additional isomers, mutually rotamers, in which terminal NH_2 groups (isomer **XII**) or carbonyl groups (isomer **X**) form six-membered rings upon coordination. Two other isomers, **IX** and **XI**, originate from the asymmetrical combinations of side-chain conformations of isomers **I**, **X**, and **XII** and are also rotamers. Of course, the mixing of isomers **IX** and **XI** is also possible, but the resulting isomer is not shown in Figure 2 because it has an unreasonably high energy and was highly distorted after optimization of its geometry. Finally, isomer **IV** is in a TPRS-7 environment, while isomers **V** and **VI** correspond to OCF-7.

Even though there is the likelihood of formation of each isomer, it has been experimentally confirmed that the $H_n$dapsox ligand always forms isomer **I** (PBPY-7) complexes with Mn^{II},[28] Fe^{III},[31,32] Fe^{II},[29] and Co^{II}.[30,33] Whenever a different ground state is possible, high spin is always observed. In order to elucidate the factors that govern this structural preference, we performed DFT calculations for all of the above-mentioned isomers (**I**−**XII**) of $[M(H_n\text{dapsox})(H_2O)_2]^q$ to examine their relative stability (see Figure 2), although some of them cannot be experimentally achieved. The apical position can be occupied with different molecules, depending on the nature of the solvent;[60] hence, for this study we modeled the apical coordination sphere with two molecules of water.

For $[Mn^{II}(\text{dapsox})(H_2O)_2]$, isomer **I** is the most stable one (see Figure 2), in which dapsox is coordinated in a symmetrical pentadentate mode through pyridine, two azomethyne (imine) nitrogen atoms, and two α-oxyazine oxygen atoms. The least stable structure corresponds to the isomer **XII** (PBPY-7) because of the coordination of two amide nitrogen atoms and the formation of two six-membered rings. The origin of the different stabilities for the two OCF-7 isomers (**V** and **VI**) can be found in the distinctive ligator atoms and the formation of a six-membered ring in isomer **VI**. Isomers **II** and **III**, obtained by outer amide rotation, have stability similar to that of isomer **I** because the high conjugation in the equatorial plane is preserved. All other isomers are much higher in energy. We were unable to obtain the TPRS-7 coordination (isomer **IV**) because of the structure of the ligand and the presence of strong hydrogen bonds between the two neighboring water molecules. The combination of these two effects caused the transition-metal complex to completely change conformation, and therefore the relative energy cannot be shown in Figure 2. This trend has been observed for all investigated $[M(H_n\text{dapsox})(H_2O)_2]^q$ complexes with other metals; see Table S1 in the Supporting Information. It is noteworthy that the geometries of the calculated structures of isomer **I** are in excellent agreement with those of similar structures characterized by X-ray.[29−31] Selected bond lengths and valence angles are collected and compared in Table S2 in the Supporting Information for corresponding structures, while the superposition of some of the crystal structures[29−31] and structures computed at the LDA level are presented in Figure 3. This figure shows the large coherence between the optimized and X-ray structures, which is the confirmation that LDA tends to give good geometries for coordination compounds.[67,74−76]

Because PBPY-7 and OCF-7 (isomers **I** and **V**, respectively, in Figure 2) are the most representative examples of coordination number 7, the following detailed discussion will

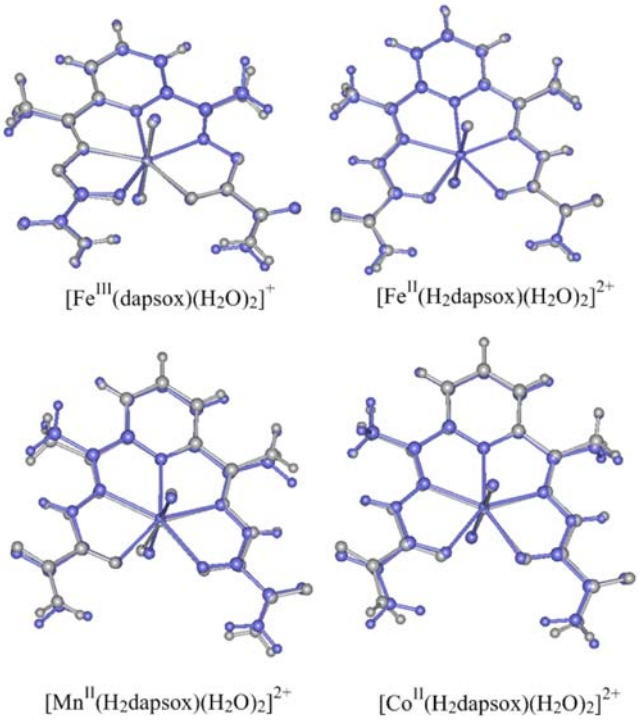

Figure 3. Overlays of available experimental X-ray- (gray) with LDA-optimized (light blue) global minimum structures of $[Fe^{III}(dapsox)(H_2O)_2]^+$, $[Fe^{II}(H_2dapsox)(H_2O)_2]^{2+}$, $[Mn^{II}(H_2dapsox)(H_2O)_2]^{2+}$, and $[Co^{II}(H_2dapsox)(H_2O)_2]^{2+}$.

be focused only on them; a full report of the energies of all other isomers with the different metal ions is given in Table S1 in the Supporting Information.

The influence of ligand deprotonation and the nature of the central metal ion on the stability of isomers **I** and **V** is presented in Table 1 for Mn^{II}, Fe^{III}, Fe^{II}, Co^{II}, and Zn^{II}. Additionally, we studied also the same types of complexes with Ni^{II} in order to rationalize experimental findings that reveal another type of coordination with this metal ion. The differences in energy for isomers **I** and **V** are observed within a range of a few kilocalories per mole (see Table 1), and in some isolated cases, the order of stability depends on the choice of the XC functional. The largest differences are found between LDA, on the one hand, and OPBE, SSB-D, and S12g, on the other hand (in all cases using LDA geometries). However, it is well-known that LDA has a very poor performance considering energies of d-block metal (TM) complexes,[77] in contrast to the geometries and vibrational frequencies of coordination compounds for which it does give accurate results.[67,74−76] Therefore, the relative energies obtained at LDA will not be further discussed. With the LDA/GGA functionals, isomer **I** is always found to be the most stable one, irrespective of the charge on the ligand and the nature of the central metal ion, except in the cases of $[Zn^{II}(Hdapsox)(H_2O)_2]^+$ and $[Zn^{II}(H_2dapsox)(H_2O)_2]^{+2}$. For these two cases, OPBE predicts OCF-7 (isomer **V**) to be the most stable isomeric structure, while SSB-D and S12g favor isomer **I**. However, the differences obtained with SSB-D and S12g are also quite smaller than those for the other d-block metal systems. To be certain that these results are not affected by the use of LDA geometries, we also used OPBE geometries, which led to the same conclusions (see Table S3 in the Supporting Information). Therefore, it is again shown that it is indeed valid to be

Table 1. Relative Energies (kcal·mol^{-1})[a] of Isomers I and V (See Figure 2) for Different 3d Metal Ions in the High-Spin State

3d metal ion	ligand	expt obsd	isomer	LDA	OPBE	SSB-D	S12g
Mn^{II}	dapsox		**I**	0	0	0	0
			V	1.7	3.5	5.0	5.1
	Hdapsox		**I**	0	0	0	0
			V	0.1	1.9	4.8	4.0
	H_2dapsox	ref 28	**I**	0	0	0	0
			V	−0.7	5.4	7.9	7.8
Fe^{III}	dapsox	ref 35	**I**	0	0	0	0
			V	−2.1	5.2	7.2	6.6
	Hdapsox	ref 32	**I**	0	0	0	0
			V	2.3	4.9	8.2	6.5
	H_2dapsox		**I**	0	0	0	0
			V	4.2	8.9	11.2	10.6
Fe^{II}	dapsox		**I**	0	0	0	0
			V	1.7	0.8	4.4	3.7
	Hdapsox		**I**	0	0	0	0
			V	0.1	3.6	6.6	5.3
	H_2dapsox	ref 29	**I**	0	0	0	0
			V	3.1	4.2	7.8	6.9
Co^{II}	dapsox	ref 30	**I**	0	0	0	0
			V	−0.2	0.2	0.6	0.6
	Hdapsox	ref 30	**I**	0	0	0	0
			V	−2.3	0.5	3.2	1.8
	H_2dapsox	ref 33	**I**	0	0	0	0
			V	1.3	4.0	8.1	6.5
Zn^{II}	dapsox		**I**	0	0	0	0
			V	14.6	4.4	6.4	6.9
	Hdapsox		**I**	0	0	0	0
			V	3.6	−2.0	3.4	2.1
	H_2dapsox	ref 28	**I**	0	0	0	0
			V	−0.4	−4.7	1.0	0.5

[a] Single-point energies with the TZP basis set, on LDA/TZP geometries.

using GGA functionals for the energy obtained in a single-point fashion on LDA geometries.

While with Mn^{II}, Fe^{III}, Fe^{II}, Co^{II}, and Zn^{II} seven-coordination is always found to be the stable one, attempts to model seven-coordinated structures with Ni^{II} and $H_n$dapsox ligands failed, resulting in an OC-6 geometry, even if we started from a PBPY-7 environment. The calculated geometry resembles the OCF-7 coordination, but one oxygen that lies on the face of the octahedron is sufficiently far away from nickel (3.16 Å) that it cannot be considered as a bond. This is in agreement with experimental findings, which hinted at the infeasibility of obtaining PBPY-7 structures for Ni^{II} with the dapsox ligand. In an ideal PBPY-7 geometry (D_{5h} symmetry) for high-spin nickel(II) complexes, e_2' orbitals are unequally populated[73] and prone to Jahn−Teller[78] distortion. In the resulting lower symmetry, like in the present case, the degeneracy is lifted, so the octahedral geometry (OC-6) in the $[Ni^{II}(dapsox)]$ complex can be explained as the result of a pseudo-Jahn−Teller effect[79] operating on the PBPY-7 environment, which leads to structural distortion.[27] The results obtained for the two isomers of Ni^{II} are shown in Table 2; they differ in the size of the chelate ring upon coordination and resemble isomers **V** and **VI** of the seven-coordinated environment from Figure 2 (differing from these because of the six-coordination, vide supra),

dx.doi.org/10.1021/ic401752n | Inorg. Chem. 2013, 52, 13415−13423

Table 2. Relative Energies (kcal·mol^{-1})[a] of Isomers V* and VI* for Nickel(II) Complexes[b] in the High-Spin State

TM ion	ligand	isomer	LDA	OPBE	SSB-D	S12g
Ni^{II}	dapsox	**V***	0	0	0	0
		VI*	−4.9	−0.4	−6.4	−4.5
	Hdapsox	**V***	0	0	0	0
		VI*	−9.1	−3.2	−7.7	−6.6

[a]Single-point energies with the TZP basis set, on LDA/TZP geometries. [b]The coordinations **V*** and **VI*** resemble those of isomers **V** and **VI** shown in Figure 2 (see the text).

respectively. Isomer **VI*** is the most stable one with both Hdapsox and dapsox, while isomer **VI*** cannot be formed with H_2dapsox.

As expected, structures with the H_2dapsox ligand are less distorted in comparison with its mono- and dianionic analogues because of weaker intermolecular hydrogen bonds; see Figure 4. In all $[M(dapsox)(H_2O)_2]^q$ complexes, the water molecules are oriented in order to form strong intermolecular hydrogen bonds, while in the complexes with H_2dapsox, the hydrogen bonds are much weaker because of the different orientations of water ligands.

Spin-State Energies of Seven-Coordinate Complexes. The effect of (de)protonation of the coordinated acylhydrazone polydentate ligands on the ligand-field strength and spin state of 3d-block metal ions, and thus on the stability of the PBPY-7 geometry, was only empirically approached in the literature:[27] the high-spin state was experimentally found to be the ground state in all investigated complexes.[28−33] As a result of our interest in both the coordination chemistry of 2,6-diacetylpyridine hydrazones and 3d metal seven-coordinate complexes[27−36] and an accurate theoretical description of spin state energetics,[14,15,38,67] here we performed DFT calculations for a systematic investigation of the spin-state splitting in these complexes. We studied $[MH_n dapsox(H_2O)_2]^q$, M = Mn^{II}, Fe^{III}, Fe^{II}, Co^{II}, and Ni^{II}, with the aim of examining how the degree of (de)protonation and the nature of the central metal ion affects spin-state preferences.

The accurate description of spin states in transition-metal complexes by means of DFT has been the focus of many studies in the past decade,[13−15,38,67,80−82] from which emerged a number of preferred density functionals (B3LYP*,[48,83−86] OPBE,[38,46,47,52,87] TPSSh,[56,88,89] M06-L,[90,91] SSB-D,[14,54,67,92] and S12g[55]), and still presents a challenge.[14] Hereby, we decided to use OPBE, SSB-D, and S12g[14,38,55,67] because of the proven accuracy for these types of problems and added solvent effects[72] through the COSMO dielectric continuum model[68,69,71] that can mimic small electrostatic perturbation from the environment. Our theoretical findings, which are in accordance with experimental data, suggest that the high-spin configuration is favored for all investigated complexes in the PBPY-7 environment with OPBE, SSB-D, and S12g. There are, however, two exceptions: for $[Co^{II}(Hdapsox)(H_2O)_2]^+$ and $[Co^{II}(dapsox)(H_2O)_2]$, OPBE and S12g predict a low spin state, while the SSB-D functional was able to capture the experimentally observed high-spin ground state (see Tables 3 and S4 in the Supporting Information). Note that these are electronic energies, without zero-point energies or entropy effects, both of which favor high-spin states.[93] Finally, it should be noted that similar results were obtained when we used either LDA (Table 3) or OPBE (Table S5 in the Supporting Information) geometries.

Neither the nature of the central metal ions nor the degree of deprotonation affects the stability ordering of the isomers; however, this cannot be said for the spin states. Interestingly, during the optimization of low-spin states, the structures distort from a PBPY-7 geometry toward the isomeric structure OCF-7 (or in some cases even to OC-6), which becomes the global minimum on the potential energy surface. This is an interesting example where the spin state can change the relative stability of isomers because a change of the spin state (of one and the same complex) is usually accompanied only with changes in bond lengths.[94−97] Again, Ni^{II} is a special case, where the triplet state is in an octahedral environment, while the singlet state distorts toward square-pyramidal geometry, corroborating experimental observations.[35]

A closer look at the MOs (see Figure 5) helps to explain our findings for the different coordination modes. In all seven-coordinated complexes, MOs that originated from d metal orbitals are quite similar in shape (see Figure S1 in the Supporting Information). The lowest two MOs are π-antibonding with respect to the oxygen atom of the dapsox ligand; the third MO is clearly σ-antibonding, with significant contribution of oxygen p orbitals, while the highest two MOs are nonbonding with respect to the oxygen atoms. According to the obtained results, the high-spin configuration will always favor the formation of a bond between the central metal and the oxygen atom in the equatorial plane, except for nickel(II) complexes. Complexes with a d^5 high-spin electronic configuration, i.e., $[Fe^{III}(H_2dapsox)(H_2O)_2]^{3+}$ and $[Mn^{II}(H_2dapsox)(H_2O)_2]^{2+}$, possess one unpaired electron in each MO. In contrast, in the low-spin state, one unpaired electron is placed in the σ-antibonding MO, but the π-antibonding orbitals are now fully occupied, which leads to rupture of the $M-O_{eq}$ bond. Something similar happens for the $[Fe^{II}(H_2dapsox)(H_2O)_2]^{2+}$ complex with a d^6 electronic configuration, which has four unpaired electrons in the high-

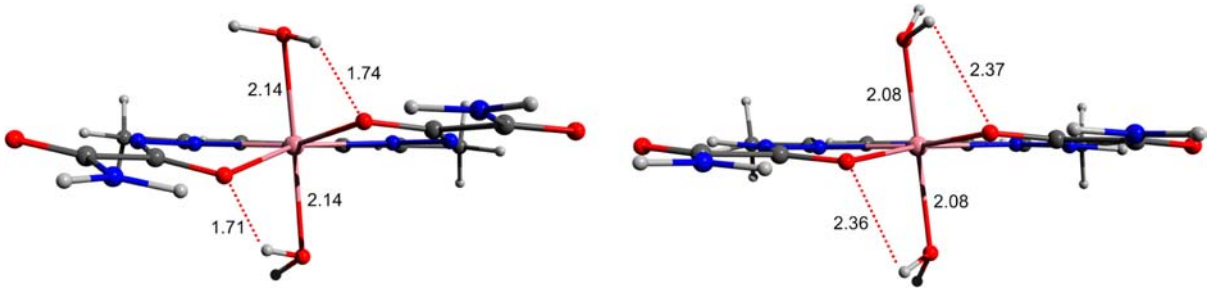

Figure 4. Structures of $[Co^{II}(dapsox)(H_2O)_2]$ (left) and $[Co^{II}(H_2dapsox)(H_2O)_2]^{2+}$ (right) with depicted bonds. Bond lengths are given in angstroms.

dx.doi.org/10.1021/ic401752n | Inorg. Chem. 2013, 52, 13415−13423

Table 3. Relative Spin-State Energies (kcal·mol^{-1})[a] for Some Metal Complexes with H$_n$dapsox Ligands

		OPBE			OPBE/COSMO			SSB-D			S12g		
	spin state	LS	IS	HS	LS	IS	HS	LS	IS	HS	LS	IS	HS
Mn^{II}	$[Mn^{II}(H_2dapsox)(H_2O)_2]^{2+}$	45.2	33.1	0	43.2	33.2	0	52.7	37.7	0	42.3	30.2	0
	$[Mn^{II}(Hdapsox)(H_2O)_2]^{+}$	25.9	12.6	0	27.4	14.8	0	33.5	16.9	0	23.6	10.7	0
	$[Mn^{II}(dapsox)(H_2O)_2]$	21.1	12.9	0	24.9	14.9	0	28.9	19.3	0	19.0	12.9	0
Fe^{III}	$[Fe^{III}(H_2dapsox)(H_2O)_2]^{3+}$	17.4	23.8	0	24.0	22.3	0	29.3	23.7	0	20.8	22.3	0
	$[Fe^{III}(Hdapsox)(H_2O)_2]^{2+}$	14.4	13.4	0	15.9	16.2	0	25.6	20.5	0	17.5	15.8	0
	$[Fe^{III}(dapsox)(H_2O)_2]^{+}$	12.4	12.0	0	15.8	17.1	0	23.8	18.9	0	15.5	14.1	0
Fe^{II}	$[Fe^{II}(H_2dapsox)(H_2O)_2]^{2+}$	17.8	32.7	0	15.7	29.4	0	29.5	34.8	0	22.2	32.0	0
	$[Fe^{II}(Hdapsox)(H_2O)_2]^{+}$	12.0	8.6	0	10.1	9.4	0	24.8	16.6	0	17.4	12.1	0
	$[Fe^{II}(dapsox)(H_2O)_2]$	7.5	9.6	0	5.3	10.1	0	17.7	16.9	0	11.4	12.5	0
Co^{II}	$[Co^{II}(H_2dapsox)(H_2O)_2]^{2+}$	2.1		0	5.5		0	15.1		0	8.4		0
	$[Co^{II}(Hdapsox)(H_2O)_2]^{+}$	−8.1		0	−5.4		0	1.9		0	−3.8		0
	$[Co^{II}(dapsox)\ (H_2O)_2]$	−7.8		0	−6.7		0	2.5		0	−3.1		0

[a]Single-point energies with a TZP basis set, on LDA/TZP geometries; LS = low spin, IS = intermediate spin, HS = high spin.

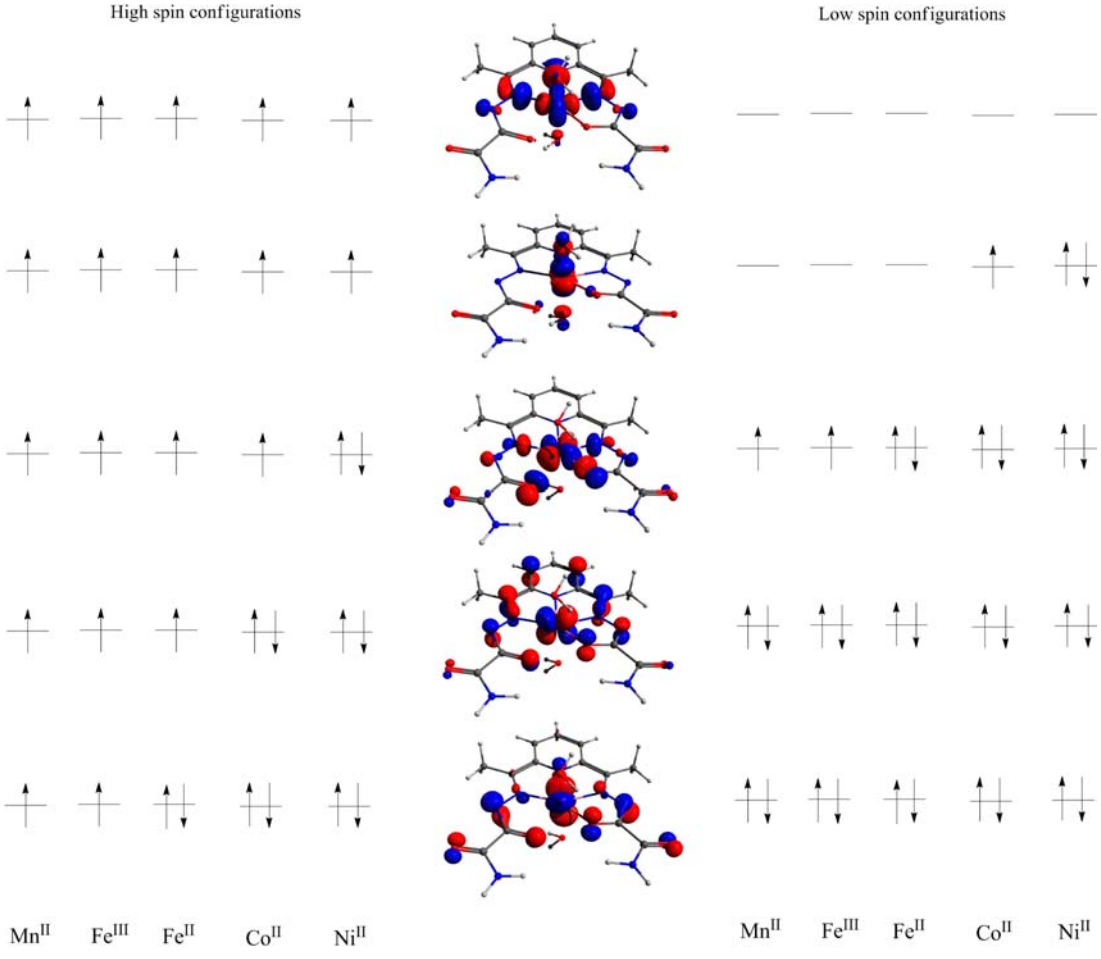

Figure 5. Representation of MOs for $[MH_ndapsox(H_2O)_2]^q$, where q = 0, 1, 2, 3, n = 0, 1, 2, and M = Mn^{II}, Fe^{III}, Fe^{II}, Co^{II}, Ni^{II}. Graphical 3D representations of the MOs (middle) are obtained for $[Co^{II}(dapsox)(H_2O)_2]$ in the high-spin state (see also Figure S1 in the Supporting Information).

spin state. These unpaired electrons are placed in the highest-lying π-antibonding, in a σ-antibonding and two nonbonding MOs. Instead, in the low-spin state, two π-antibonding and the σ-antibonding MOs are doubly occupied; hence, the breaking of the M−O_{eq} bond is a consequence of both π- and σ-antibonding interactions. In the case of $[Co^{II}(H_2dapsox)(H_2O)_2]^{2+}$, both high-and low-spin states have doubly occupied π-antibonding MOs (Figure 5); hence, the difference in geometry between the two states results almost completely from σ-antibonding interactions. Finally, $[Ni^{II}(H_2dapsox)(H_2O)_2]^{2+}$ has doubly occupied π- and σ-antibonding MOs in high- and low-spin states; thus, in both cases, the PBPY-7 coordination cannot be the preferred geometry (as is indeed observed in our calculations and in previous experiments).

Five-Coordinated Complexes. Because H$_n$dapsox has many potential ligator atoms, it can be coordinated not only

dx.doi.org/10.1021/ic401752n | Inorg. Chem. 2013, 52, 13415−13423

as a pentadentate but also as a tetradentate ligand, forming complexes with coordination number 5. It is well-known that complexes with coordination number 5 can form trigonal-bipyramidal (TBPY-5) and SPY-5 geometries. Bearing in mind the rigidity of the mono- and dianionic forms of the ligand upon coordination in the equatorial plane, the formation of the TBPY-5 isomer is not possible, and our discussion will be limited to SPY-5 complexes. Furthermore, because of the presence of the two additional protons at the nitrogen atoms, SPY-5 cannot be formed with H_2dapsox. To the best of our knowledge, only $[Cu^{II}(dapsox)H_2O]$ and $[Cu^{II}(Hdapsox)H_2O]^+$ complexes were determined crystallographically,[32,36] while $[Fe^{III}(dapsox)Cl]$ was synthesized but not characterized crystallographically.[34] The two crystal structures of the copper complexes have different conformations; i.e., the uncoordinated pending arm of the ligand lies respectively above and below the equatorial plane in $[Cu^{II}(dapsox)H_2O]$ and $[Cu^{II}(Hdapsox)H_2O]^+$. Interestingly, previous experimental work had shown that the intermediate spin state ($S = {}^3/_2$) is the electronic ground state for the SPY-5 complex of $[Fe^{III}(dapsox)Cl]$.[34] In order to study this surprising (and unusual) spin ground state in more detail, we performed DFT calculations for $[M(H_ndapsox)L]^q$, where M = Fe^{III}, Cu^{II} and L = H_2O, Cl^-. The DFT-optimized geometries of $[Cu^{II}(dapsox)H_2O]$ and $[Cu^{II}(Hdapsox)H_2O]^+$ are in excellent agreement with the X-ray structures (see Figure 6), giving us considerable confidence about the reliability of the computed structure of the $[Fe^{III}(dapsox)Cl]$ complex as well. Selected average bond lengths and valence angles for DFT-optimized and X-ray structures are tabulated in Table S6 in the Supporting Information.

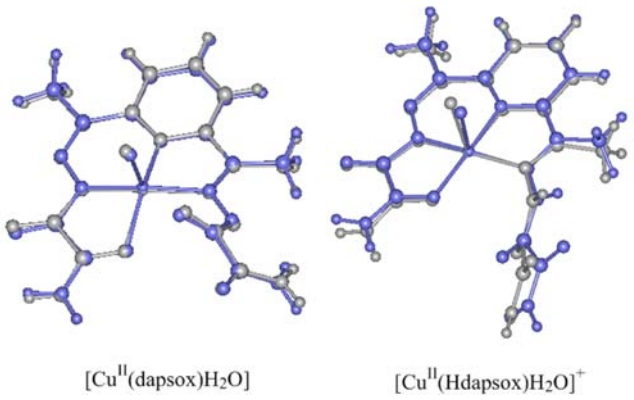

Figure 6. Superposition of available experimental X-ray- (gray) with LDA-optimized (light blue) global minimum structures of $[Cu^{II}(dapsox)H_2O]$ and $[Cu^{II}(Hdapsox)H_2O]^+$.

Spin-State Energies of Five-Coordinated Complexes. The only synthesized five-coordinated complex with $H_n$dapsox ligands that has the possibility of multiple spin states is $[Fe^{III}(dapsox)Cl]$. As already mentioned above, this complex has been well characterized, and the measurement of its magnetic momentum with EPR spectra at different temperatures clearly indicated a rarely observed intermediate spin state.[34] Motivated by this interesting result, we have performed DFT calculations for obtaining the spin-state splitting in $[Fe^{III}(H_ndapsox)L]$ with n = 0, 1 and L = H_2O, Cl^-, with the aim of examining how the degree of deprotonation and the nature of the apical ligand affect the spin-state preferences. The results are shown in Table 4.

In the case of $[Fe^{III}(dapsox)Cl]$, all three functionals (OPBE, SSB-D, and S12g) indicated correctly the intermediate spin ground state, in agreement with the intriguing experimental results.[34] In contrast, for the Hdapsox ligand (not isolated experimentally), a high-spin state is predicted by all methods, but the splitting with the intermediate spin is greatly reduced (to ca. 1−6 kcal·mol^{-1}, depending on the functional and whether solvent effects have been taken into account). Hence, in the continuous compromise between larger orbital splittings (preferring low spin) and enhanced exchange interactions[98] (favoring high spin), in this latter case, the exchange interactions are more important.

Examination of the complexes with a water molecule in the apical position, $[Fe^{III}(dapsox)H_2O]^+$ and $[Fe^{III}(Hdapsox)H_2O]^{2+}$, showed that the intermediate spin is favored by OPBE and S12g, while SSB-D predicts a high-spin configuration with Hdapsox but an intermediate spin with dapsox (see Table 4). It is worth mentioning that in the case of $[Fe^{III}(dapsox)H_2O]^+$ all three methods predict that the high and intermediate spin states are very close in energy, thereby indicating that it can be considered a potential candidate for spin-crossover systems. It should be noted that these conclusions were not affected either by the addition of solvent effects with COSMO (Table S7 in the Supporting Information) or by optimization of the geometry at OPBE/TZP (Table S8 in the Supporting Information).

CONCLUSIONS

The electronic structure and stereochemistry of acylhydrazone complexes with Mn^{II}, Fe^{III}, Fe^{II}, Co^{II}, Ni^{II}, Cu^{II}, and Zn^{II} were studied by means of DFT. Some of these complexes exhibit an unusual PBPY-7 geometry, which has rarely been studied until now. Because H_2dapsox and its anionic forms have 11 potential donor atoms and therefore a versatile coordination behavior with respect to the ligator atoms, 12 possible isomeric structures were examined in the seven-coordinated environment. Isomer **I** was obtained experimentally always, regardless of the different possibilities of ligand coordination and the large number of possible isomers. Our theoretical investigations have shown that the geometry of isomer **I**, in the high-spin configuration, is in excellent agreement with the X-ray

Table 4. Relative Spin-State Energies (kcal·mol^{-1})[a] for Five-Coordinated Fe^{III} with Hdapsox and dapsox Ligands

	OPBE			OPBE/COSMO			SSB-D			S12g		
spin state	LS	IS	HS	LS	IS	HS	LS	IS	HS	LS	IS	HS
$[Fe^{III}(dapsox)Cl]$	7.6	−9.7	0	8.1	−10.5	0	11.1	−6.6	0	3.3	−11.9	0
$[Fe^{III}(Hdapsox)Cl]^+$	13.6	2.6	0	11.7	0.6	0	19.8	5.6	0	14.0	2.2	0
$[Fe^{III}(dapsox)H_2O]^+$	3.7	−2.2	0	4.8	−1.5	0	11.9	1.8	0	5.1	−3.4	0
$[Fe^{III}(Hdapsox)H_2O]^{2+}$	8.4	−6.3	0	8.8	−6.4	0	12.3	−4.9	0	6.2	−7.8	0

[a]Single-point energies with TZP basis set, on LDA/TZP geometries; HS = high spin, IS = intermediate spin, LS = low spin.

dx.doi.org/10.1021/ic401752n | Inorg. Chem. 2013, 52, 13415−13423

structures; moreover, this isomer is found to be the most stable one, irrespective of the nature of the central metal or the charge of the ligand. The energy ordering for the other isomers was found to be clearly influenced by the types of donor atoms and the size of the chelate rings formed upon coordination.

A different situation is observed when we consider low-spin configurations of the central metal ions. Because of the different populations of bonding/antibonding orbitals, the geometry optimization of an initial PBPY-7 coordination distorts toward an OCF-7 geometry, which explains why only high-spin states are detected in a PBPY-7 environment. Furthermore, our calculations explain why Ni^{II} is not forming seven-coordinated complexes with these ligands: an octahedral polyhedral environment is found to be the most stable one, for high spin, even though the optimization was started from a different coordination number. However, nickel(II) complexes in a singlet state distort toward a SPY-5 geometry, corroborating experimental observations. This is an interesting example where the spin state can completely change the geometry of the stable species, even though usually a change of the spin state (for one and the same complex) is accompanied only by a change of bond lengths.

The intriguing experimental observation that [Fe^{III}(dapsox)-Cl] is in the intermediate spin has been confirmed by our DFT calculations, with the OPBE, SSB-D, or S12g functionals. This proves that a DFT calculation with either one of these density functionals is the method of choice for studying the spin-state diversity. As a final remark, our computational results explain all experimental findings and give deeper insight into the understanding of the chemistry of these interesting compounds, which may affect further development in the field as well as the rational design of new compounds with desired properties.

■ ASSOCIATED CONTENT

Supporting Information

Relative energies, selected bond lengths and angles, shapes of MOs, and coordinates of metal complexes. This material is available free of charge via the Internet at http://pubs.acs.org.

■ AUTHOR INFORMATION

Corresponding Authors

*E-mail: gmaja@chem.bg.ac.rs.
*E-mail: marcel.swart@icrea.cat.

Notes

The authors declare no competing financial interest.

■ ACKNOWLEDGMENTS

The following organizations are thanked for financial support: the Ministerio de Ciencia e Innovación (MICINN; Project CTQ2011-25086/BQU), the DIUE of the Generalitat de Catalunya (Project 2009SGR528, Xarxa de Referència en Química Teòrica i Computacional), and the Serbian Ministry of Education and Science (Grant 172035). Financial support from MICINN (Ministry of Science and Innovation, Spain) and the FEDER fund (European Fund for Regional Development) was provided by Grant UNGI08-4E-003.

■ REFERENCES

(1) Boyd, D. B. *Rev. Comput. Chem.* **2007**, *23*, 401−451.
(2) Xantheas, S. *Nature* **2009**, *457*, 673−674.
(3) Fantacci, S.; Amat, A.; Sgamellotti, A. *Acc. Chem. Res.* **2010**, *43*, 802−813.
(4) Rokob, T. A.; Srneca, M.; Rulíšek, L. *Dalton Trans.* **2012**, *41*, 5754−5768.
(5) Makshakova, O.; Ermakova, E. *Chem. Phys.* **2013**, *415*, 282−290.
(6) Domingo, L. R.; Saez, J. A.; Joule, J. A.; Rhyman, L.; Ramasami, P. *J. Org. Chem.* **2013**, *78*, 1621−1629.
(7) Pidlypnyi, N.; Namyslo, J. C.; Drafz, M. H. H.; Nieger, M.; Schmidt, A. *J. Org. Chem.* **2013**, *78*, 1070−1079.
(8) Tang, B.; Zhang, Y.-H.; Song, R.-J.; Tang, D.-J.; Deng, G.-B.; Wang, Z.-Q.; Xie, Y.-X.; Xia, Y.-Z.; Li, J.-H. *J. Org. Chem.* **2012**, *77*, 2837−2849.
(9) Linder, M.; Johansson, A. J.; Brinck, T. *Org. Lett.* **2012**, *14*, 118−121.
(10) Jacolot, M. J. M.; Levoin, N.; van de Weghe, P. *Org. Lett.* **2012**, *14*, 58−61.
(11) Cramer, C.; Truhlar, D. G. *Phys. Chem. Chem. Phys.* **2009**, *11*, 10757−10816.
(12) Reiher, M. *Chimia* **2009**, *63*, 140−145.
(13) Harvey, J. N. *Struct. Bonding (Berlin)* **2004**, *112*, 151−183.
(14) Swart, M. *Int. J. Quantum Chem.* **2013**, *113*, 2−7.
(15) Ghosh, A. *J. Biol. Inorg. Chem.* **2006**, *11*, 712−724.
(16) Milsmann, C.; Bothe, E.; Bill, E.; Weyhermueller, T.; Wieghardt, K. *Inorg. Chem.* **2009**, *48*, 6211−6221.
(17) Orio, M.; Philouze, C.; Jarjayes, O.; Neese, F.; Thomas, F. *Inorg. Chem.* **2010**, *49*, 646−658.
(18) Fey, N.; Harvey, J. N.; Lloyd-Jones, G. C.; Murray, P.; Orpen, A. G.; Osborne, R.; Purdie, M. *Organometallics* **2008**, *27*, 1372−1383.
(19) Praetorius, J. M.; Allen, D. P.; Wang, R.; Webb, J. D.; Grein, F.; Kennepohl, P.; Crudden, C. M. *J. Am. Chem. Soc.* **2008**, *130*, 3724−3725.
(20) Ross, A. J.; Dreiocker, F.; Schaefer, M.; Oomens, J.; Meijer, A. J. H. M.; Pickup, B. T.; Jackson, R. F. W. *J. Org. Chem.* **2011**, *76*, 1727−1734.
(21) Vaiana, L.; Regueiro-Figueroa, M.; Mato-Iglesias, M.; Platas-Iglesias, C.; Esteban-Gómez, D.; de Blas, A.; Rodriguez-Blas, T. *Inorg. Chem.* **2007**, *46*, 8271−8282.
(22) Gutman, C. T.; Guzei, I. A.; Brunold, T. C. *Inorg. Chem.* **2013**, *52*, 8909−8918.
(23) Jackson, T. A.; Gutman, C. T.; Maliekal, J.; Miller, A.-F.; Brunold, T. C. *Inorg. Chem.* **2013**, *52*, 3356−3367.
(24) Zhang, D.; Busch, D. H.; Lennon, P. L.; Weiss, R. H.; Neumann, W. L.; Riley, D. P. *Inorg. Chem.* **1998**, *37*, 956−963.
(25) Gutman, C. T.; Brunold, T. C. *Inorg. Chem.* **2012**, *51*, 12729−12737.
(26) Lieb, D.; Friedel, F. C.; Yawer, M.; Zahl, A.; Khusniyarov, M. M.; Heinemann, F. W.; Ivanović-Burmazović, I. *Inorg. Chem.* **2013**, *52*, 222−236.
(27) Ivanović-Burmazović, I.; Anđelković, K. *Adv. Inorg. Chem.* **2004**, *55*, 315−360.
(28) Šumar, M.; Ivanović-Burmazović, I.; Hodžić, I.; Andjelković, K. *Synth. React. Inorg. Met.* **2002**, *32*, 721−737.
(29) Liu, G.-F.; Filipović, M.; Heinemann, F. W.; Ivanovíc-Burmazović, I. *Inorg. Chem.* **2007**, *46*, 8825−8835.
(30) Andelković, K.; Ivanović, I.; Prelesnik, B. V.; Leovac, V. M.; Poleti, D. *Polyhedron* **1996**, *15*, 4361−4366.
(31) Andjelković, K.; Bacchi, A.; Pelizzi, G.; Jeremić, D.; Ivanović-Burmazović, I. *J. Coord. Chem.* **2002**, *55*, 1385−1392.
(32) Ivanović-Burmazović, I.; Bacchi, A.; Pelizzi, G.; Leovac, V. M.; Andjelković, K. *Polyhedron* **1999**, *18*, 119−127.
(33) Ivanović, I.; Andelković, K.; Beljanski, V.; Prelesnik, B. V.; Leovac, V. M.; Momirović, M. *J. Coord. Chem.* **1997**, *42*, 335−342.
(34) Bacchi, A.; Ivanović-Burmazović, I.; Pelizzi, G.; Andjelković, K. *Inorg. Chim. Acta* **2001**, *313*, 109−119.
(35) Pelizzi, G.; Bacchi, A.; Ivanović-Burmazović, I.; Gruden, M.; Andjelković, K. *Inorg. Chem. Commun.* **2001**, *4*, 311−314.
(36) Andelković, K.; Ivanović, I.; Niketić, S. R.; Prelesnik, B. V.; Leovac, V. M. *Polyhedron* **1997**, *16*, 4221−4228.
(37) Remacle, F.; Grandjean, F.; Long, G. *Inorg. Chem.* **2008**, *47*, 4005−4014.
(38) Swart, M. *J. Chem. Theory Comput.* **2008**, *4*, 2057−2066.

(39) Dirac, P. A. M. *Proc. R. Soc. London, A* **1931**, *123*, 714−733.
(40) Slater, J. C. *Phys. Rev.* **1951**, *81*, 385−390.
(41) Vosko, S. H.; Wilk, L.; Nusair, M. *Can. J. Phys.* **1980**, *58*, 1200−1211.
(42) Perdew, J. P.; Wang, Y. *Phys. Rev. B* **1992**, *45*, 13244−13249.
(43) Becke, A. D. *Phys. Rev. A* **1988**, *38*, 3098−3100.
(44) Perdew, J. P.; Yue, W. *Phys. Rev. B* **1986**, *33*, 8800−8802.
(45) Lee, C.; Yang, W.; Parr, R. G. *Phys. Rev. B* **1988**, *37*, 785−789.
(46) Perdew, J. P.; Burke, K.; Ernzerhof, M. *Phys. Rev. Lett.* **1996**, *77*, 3865−3868.
(47) Swart, M.; Groenhof, A. R.; Ehlers, A. W.; Lammertsma, K. *J. Phys. Chem. A* **2004**, *108*, 5479−5483.
(48) Stephens, P. J.; Devlin, F. J.; Chabalowski, C. F.; Frisch, M. J. *J. Phys. Chem.* **1994**, *45*, 11623−11627.
(49) Perdew, J. P.; Ernzerhof, M.; Burke, K. *J. Chem. Phys.* **1996**, *105*, 9982−9985.
(50) Zhao, Y.; Truhlar, D. G. *Theor. Chem. Acc.* **2008**, *120*, 215−241.
(51) Swart, M. *Inorg. Chim. Acta* **2007**, *360*, 179−189.
(52) Handy, N. C.; Cohen, A. *Mol. Phys.* **2001**, *99*, 403−412.
(53) Swart, M.; Ehlers, A. W.; Lammertsma, K. *Mol. Phys.* **2004**, *102*, 2467−2474.
(54) Swart, M.; Solà, M.; Bickelhaupt, F. M. *J. Chem. Phys.* **2009**, *131*, 094103.
(55) Swart, M. *Chem. Phys. Lett.* **2013**, *580*, 166−171.
(56) Jensen, K. P. *Inorg. Chem.* **2008**, *47*, 10357−10365.
(57) Dees, A.; Zahl, A.; Puchta, R.; van Eikema Hommes, N. J. R.; Heinemann, F. W.; Ivanović-Burmazović, I. *Inorg. Chem.* **2007**, *46*, 2459−2470.
(58) Ivanović-Burmazović, I.; Hamza, M. S. A.; van Eldik, R. *Inorg. Chem.* **2006**, *45*, 1575−1584.
(59) Sarauli, D.; Meier, R.; Liu, G.-F.; Ivanović-Burmazović, I.; van Eldik, R. *Inorg. Chem.* **2005**, *44*, 7624−7633.
(60) Sarauli, D.; Popova, V.; Zahl, A.; Puchta, R.; Ivanović-Burmazović, I. *Inorg. Chem.* **2007**, *46*, 7848−7860.
(61) Sarauli, D.; van Eldik, R.; Ivanović-Burmazović, I. *Bioinorg. React. Mech.* **2012**, *8*, 107−124.
(62) Baerends , E. J.; Autschbach, J.; Bérces, A.; Berger, J. A.; Bickelhaupt, F. M.; Bo, C.; de Boeij, P. L.; Boerrigter, P. M.; Cavallo, L.; Chong, D. P.; Deng, L.; Dickson, R. M.; Ellis, D. E.; van Faassen, M.; Fan, L.; Fischer, T. H.; Fonseca Guerra, C.; van Gisbergen, S. J. A.; Groeneveld, J. A.; Gritsenko, O. V.; Grüning, M.; Harris, F. E.; van den Hoek, P.; Jacob, C. R.; Jacobsen, H.; Jensen, L.; Kadantsev, E. S.; van Kessel, G.; Klooster, R.; Kootstra, F.; van Lenthe, E.; McCormack, D. A.; Michalak, A.; Neugebauer, J.; Nicu, V. P.; Osinga, V. P.; Patchkovskii, S.; Philipsen, P. H. T.; Post, D.; Pye, C. C.; Ravenek, W.; Romaniello, P.; Ros, P.; Schipper, P. R. T.; Schreckenbach, G.; Snijders, J. G.; Solà, M.; Swart, M.; Swerhone, D.; teVelde, G.; Vernooijs, P.; Versluis, L.; Visscher, L.; Visser, O.; Wang, F.; Wesolowski, T. A.; van Wezenbeek, E. M.; Wiesenekker, G.; Wolff, S. K.; Woo, T. K.; Yakovlev, A. L.; Ziegler, T. *ADF 2012.01*; SCM: Amsterdam, The Netherlands, 2012.
(63) Guerra, C. F.; Snijders, J. G.; teVelde, G.; Baerends, E. *Theor. Chem. Acc.* **1998**, *99*, 391−403.
(64) te Velde, G.; Bickelhaupt, F. M.; Baerends, E. J.; Fonseca Guerra, C.; van Gisbergen, S. J. A.; Snijders, J. G.; Ziegler, T. *J. Comput. Chem.* **2001**, *22*, 931−967.
(65) van Lenthe, E.; Baerends, E. J. *J. Comput. Chem.* **2003**, *24*, 1142−1156.
(66) Swart, M.; Solà, M.; Bickelhaupt, F. M. *J. Comput. Methods Sci. Eng.* **2009**, *9*, 69−77.
(67) Zlatar, M.; Gruden-Pavlović, M.; Güell, M.; Swart, M. *Phys. Chem. Chem. Phys.* **2013**, *15*, 6631−6639.
(68) Klamt, A.; Schüürmann, G. *J. Chem. Soc., Perkin Trans. 2* **1993**, 799−805.
(69) Klamt, A. *J. Phys. Chem.* **1995**, *99*, 2224−2235.
(70) Klamt, A.; Jones, V. *J. Chem. Phys.* **1996**, *105*, 9972−9981.
(71) Pye, C. C.; Ziegler, T. *Theor. Chem. Acc.* **1999**, *101*, 396−408.
(72) Swart, M.; Rösler, E.; Bickelhaupt, F. M. *Eur. J. Inorg. Chem.* **2007**, 3646−3654.
(73) Hoffmann, R.; Beier, B. F.; Muetterties, E. L.; Rossi, A. R. *Inorg. Chem.* **1977**, *16*, 511−522.
(74) Andjelković, L.; Gruden-Pavlović, M.; Daul, C.; Zlatar, M. *Int. J. Quantum Chem.* **2013**, *113*, 859−864.
(75) Bray, M. R.; Deeth, R. J.; Paget, V. J.; Sheen, P. D. *Int. J. Quantum Chem.* **1996**, *61*, 85−91.
(76) Kundu, T. K.; Bruyndonckx, R.; Daul, C.; Manoharan, P. T. *Inorg. Chem.* **1999**, *38*, 3931−3934.
(77) Deeth, R. J.; Brooke Jenkins, H. D. *J. Phys. Chem. A* **1997**, *101*, 4793−4798.
(78) Bersuker, I. B. *The Jahn−Teller Effect*; Cambridge University Press: 2006.
(79) Garcıa-Fernandez, P.; Garcıa-Lastra, J. M.; Trueba, A.; Barriuso, M. T.; Aramburu, J. A.; Moreno, M. *Phys. Rev. B* **2012**, *85*, 094110 (1−9).
(80) Costas, M.; Harvey, J. N. *Nat. Chem.* **2013**, *5*, 7−9.
(81) Tangen, E.; Conradie, J.; Ghosh, A. *Inorg. Chem.* **2005**, *44*, 8699−8706.
(82) Harvey, J. *WIREs Comput. Mol. Sci.* **2013**, *3*, online, DOI: 10.1002/wcms.1154.
(83) Reiher, M.; Salomon, O.; Hess, B. A. *Theor. Chem. Acc.* **2001**, *107*, 48−55.
(84) Reiher, M. *Inorg. Chem.* **2002**, *41*, 6928−6935.
(85) Siegbahn, P. E. M.; Blomberg, M. R. A.; Chen, S.-L. *J. Chem. Theory Comput.* **2010**, *6*, 2040−2044.
(86) Becke, A. D. *J. Chem. Phys.* **1993**, *98*, 5648−5652.
(87) Conradie, J.; Ghosh, A. *J. Phys. Chem. B* **2007**, *111*, 12621−12624.
(88) Staroverov, V. N.; Scuseria, G. E.; Tao, J.; Perdew, J. P. *J. Chem. Phys.* **2003**, *119*, 12129−12137.
(89) Tao, J. M.; Perdew, J. P.; Staroverov, V. N.; Scuseria, G. E. *Phys. Rev. Lett.* **2003**, *91*, 146401 (1−4).
(90) Zhao, Y.; Truhlar, D. G. *J. Chem. Phys.* **2006**, *125*, 194101.
(91) Swart, M.; Güell, M.; Solà, M. Accurate description of spin states and its implications for catalysis. In *Quantum Biochemistry: Electronic structure and biological activity*; Matta, C. F., Ed.; Wiley-VCH: Weinheim, Germany, 2010; Vol. 2, pp 551−583.
(92) Swart, M. *Chem. Commun.* **2013**, *49*, 6650−6652.
(93) Kepp, K. P. *Coord. Chem. Rev.* **2013**, *257*, 196−209.
(94) Gaspar, A. B.; Ksenofontov, V.; Reiman, S.; Gütlich, P.; Thompson, A. L.; Goeta, A. E.; Muñoz, M. C.; Real, J. A. *Chem.—Eur. J.* **2006**, *12*, 9289−9298.
(95) Gütlich, P.; Gaspar, A. B.; Garcia, Y. *Beilstein J. Org. Chem.* **2013**, *9*, 342−391.
(96) McGrath, C. M.; O'Connor, C. J.; Sangregorio, C.; Seddon, J. M. W.; Sinn, E.; Sowrey, F. E.; Young, N. A. *Inorg. Chem. Commun.* **1999**, *2*, 536−539.
(97) Yan, J.-Q.; Zhou, J.-S.; Goodenough, J. B. *Phys. Rev. B* **2004**, *69*, 1−6.
(98) Shaik, S.; Chen, H.; Janardanan, D. *Nat. Chem.* **2011**, *3*, 19−27.